frontiers | Frontiers in Energy Research

TYPE Original Research
PUBLISHED 26 September 2024
DOI 10.3389/fenrg.2024.1467637

OPEN ACCESS

EDITED BY
Soumya Ranjan Das,
Parala Maharaja Engineering College (P.M.E.C), India

REVIEWED BY
Hemanta Kumar Sahu,
VIT University, India
Bijayananda Patnaik,
National Institute of Technology Raipur, India

*CORRESPONDENCE
Umamani Subudhi,
umamani@iiit-bh.ac.in

RECEIVED 20 July 2024
ACCEPTED 30 August 2024
PUBLISHED 26 September 2024

CITATION
Pati SS and Subudhi U (2024) Robust-momentum-learning-rate-based adaptive fractional-order least mean squares approach for power system frequency estimation using chaotic Harris hawks optimization.
Front. Energy Res. 12:1467637.
doi: 10.3389/fenrg.2024.1467637

Robust-momentum-learning-rate-based adaptive fractional-order least mean squares approach for power system frequency estimation using chaotic Harris hawks optimization

Subhranshu Sekhar Pati and Umamani Subudhi*

Department of Electrical Engineering, International Institute of Information Technology, Bhubaneswar, India

A novel robust adaptive technique is proposed to estimate the instantaneous power system frequency using a momentum-learning-control-rate-based fractional-order least mean squares approach with enhanced Harris hawks optimization. The adaptive estimation comprises two modules, where the first part involves the design of the momentum-learning-control-term-based fractional-order least mean squares algorithm and second part focuses on parameter tuning of the algorithm through enhanced Harris hawks optimization incorporating chaotic mapping and opposition-based learning. This integration yields a robust and automated adaptive algorithm for frequency estimation with superior performance compared to traditional transform-based techniques, particularly in the presence of noise. The proposed method excels in scenarios where the estimator should manage multiple variables, including step size, fractional-order step constants, and momentum learning control terms. Moreover, it facilitates accurate power frequency estimation for real signals in multiarea power systems or microgrids. To validate the efficacy of the algorithm, computer-simulated data representing step and ramp changes in the frequency were processed. Additionally, the algorithm was tested with signals derived from a multiple-control-area, multisource renewable-based power system. Detailed comparative results were obtained and verified through MATLAB simulations and real-time experimental setup, demonstrating the superior performance of the adaptive model.

KEYWORDS

frequency estimation, improved momentum learning rate, fractional least mean squares algorithm, Harris hawks optimization, chaotic map, opposition-based leaning

1 Introduction

1.1 Background and literature review

Frequency is an index of the operating practices of a power system and is one of its most important power quality parameters (Zhao et al., 2019). The frequency of a power system can deviate from its nominal value by an amount within a certain tolerance level; any deviation beyond the predetermined tolerance level is detrimental to the system and is a sign of abnormal system operating conditions that necessitate remedial actions. These problems include generation–load imbalances and improper functioning of the power system. An inaccurate frequency parameter in a power network can lead to insufficient load shedding via frequency relays, which may ultimately result in a catastrophic breakdown of the grid (Bose, 2020; Alhelou et al., 2019); moreover, the power signal would no longer be static owing to the presence of noise, voltage imbalances, and harmonics, among others. Therefore, accurate frequency estimations of dynamic signals are necessary in power system operations and have garnered considerable attention from researchers.

In reality, numerous strategies have been proposed over the years to estimate the power system frequency. The time between two zero crossings is the basis of the traditional approach (Friedman, 1994; Zhang et al., 2017), which assumes that the power system voltage is entirely sinusoidal and that the interval between two zero crossings is a measure of the grid frequency. These techniques are ineffective when dealing with dynamic changes and in the presence of harmonics and excessive noise. Several approaches have been proposed on the basis of phase-locked loops (Han et al., 2015; Xu and Song, 2020; Li et al., 2019), least-squares adaptive filtering (Zhang et al., 2019; Martinek et al., 2019), recursive total least-squares approach (Avalos et al., 2021), adaptive notch filters (Man et al., 2021; Pan et al., 2021), and extended Kalman filters (Mojiri et al., 2007; Xie et al., 2023), which have been investigated extensively for estimation purposes; such approaches have the potential to overcome the aforementioned restrictions. However, most of the currently used techniques focus on voltage measurements in single-phase systems or make assumptions about balanced-power system states. Owing to the possibility of imbalance, single-phase signals cannot be used to accurately measure the system frequencies in three-phase systems (Wold and Wilches-Bernal, 2021); hence, knowledge of all three phases must be considered for reliable and robust frequency estimations.

Furthermore, advancements in fractional calculus approaches have enabled more research activities in numerous domains, such as biomedical engineering, fluid mechanics, optics, computer vision, electrochemistry, control systems, and signal processing (Tan et al., 2015). In this context, newer fractional adaptive algorithms have inherited their concepts from fractional calculus and incorporated adaptive algorithms (Naik et al., 2024). For instance, the fractional least mean squares (FLMS) identification method that adds a percentage of each gradient based on the value of a forgetting factor was established by applying the ideas of fractional calculus; consequently, better convergence is obtained compared to the original least mean squares (LMS) algorithm. By using a sliding window that considers the past input parameters in addition to the present parameters, the convergence qualities of the FLMS approach are further enhanced (Aslam et al., 2017). Chaudhary et al. (2015) presented a scheme that simply incorporates a partial component of the gradient in the weight vector equation to decrease the computing complexity. The total convergence is unaffected by the elimination of the integer-order gradient and retention of only the fractional component, but the computational complexity is decreased by the integer-order gradient; as the fractional order approaches unity, the convergence rate increases. The fractional orders employed in algorithms thus far are in the range of (0,1), where a higher fractional order may also increase the steady-state error, as reported by Cheng et al. (2017); researchers have discovered that the rapidity and accuracy have the same characteristics as those of the original FLMS (Chaudhary et al., 2021) and modified LMS (Bershad et al., 2017). The above discussion demonstrates that several LMS variations have been extended to fractional order and that their attributes have been investigated. These works also include the momentum term in FLMS (mFLMS) in parameter estimation modeling of sinusoidal signals (Sharma et al., 1998). The convergence rate of the mFLMS increases as the weight update equation is revised to include a percentage change of the previously calculated gradients and an additional learning rate (Zubair et al., 2018). Hence, the momentum-learning-rate-based FLMS technique is a perfect candidate for identification and estimation studies; the widespread advantages of this algorithm warrant further investigations, particularly in the context of power frequency estimation. In the present work, the concept of the momentum-based FLMS algorithm is used for power system frequency estimation.

Several constants are also known to be associated with the weight update equation. For instance, the mFLMS algorithm considered in this study has three parameters, namely the step size, fractional-order step constants, and momentum learning control terms. Moreover, the values of these parameters are in the range of 0–1 and considered manually or empirically, which may result in drastic errors in the final outcome. There are no available roadmaps that provide robust methods to consider appropriate values for the variables. Therefore, optimization algorithms can be employed in these scenarios to identify the optimal values of each of the constants. The optimization algorithms are computational in nature and search for constant values in global as well as local space vectors to achieve the least possible errors (Kanoongo and Giri, 2023). Such algorithms have also been shown to produce encouraging results for noise cancellation, adaptive filtering, controller tuning, computer vision, and other applications (Alhussan et al., 2023). Some of the commonly used optimization algorithms include gray wolf optimization (GWO), genetic algorithm (GA), bat optimization, teaching-learning-based optimization (TLBO), fuzzy rules, cuckoo search algorithm (CSA), and flower pollination algorithm. A more effective approach called the Harris hawks optimization (HHO) algorithm was suggested recently and has been shown to be very effective for multivariable optimization problems (Heidari et al., 2019). The innovative HHO algorithm was developed in response to the chasing behaviors of Harris hawks; by simulating the pursuit of prey, sudden attacks, and various attack strategies used by Harris hawks, the algorithm has been applied to six well-known benchmark engineering problems, including the formulation of the 3-bar truss, tension/compression spring design, pressure vessel requirement, welded beam design, rolling element design, and multiplate disc

clutch brake problems. The HHO is prone to local optimum and slow convergence problems, just like any other natural heuristic algorithm (Alabool et al., 2021). Therefore, there is still scope for development in the HHO, where the solution involves incorporating chaotic-based functions (Shehab et al., 2022). In addition, it has been demonstrated that adding a chaotic function to the optimizer can significantly affect the algorithm's ability to perform local and global searches (Menesy et al., 2019). Consequently, the chaotic map-based HHO (iHHO) method was considered in this study along with momentum-learning-rate-based FLMS to achieve better accuracy and faster convergence than existing mFLMS algorithms; named as improved momentum-learning- rate-based FLMS (imFLMS) estimation algorithm.

1.2 Motivation and objective of the investigation

As discussed above, the fractional-order LMS algorithm provides significant benefits over the integer-order LMS algorithm for power frequency estimation, with faster convergence rates and improved accuracies, especially in environments with high degrees of noise. Furthermore, considering that the momentum learning control term in the FLMS algorithm enables more precise adjustments, enhanced resistance to noise and capacity to adapt to dynamic signal conditions are obtained. This adaptability leads to reduced steady-state errors and improved stability across a wider spectrum of operating conditions. Furthermore, the momentum learning control terms in the FLMS algorithm entail multiple parameters such as step size, fractional-order step constants, and momentum learning control terms, all of which range from 0 to 1 and are chosen manually or empirically, which can potentially cause significant errors. Optimization algorithms are used to determine the optimal values for these parameters computationally, thereby minimizing errors by exploring the global and local space vectors (Chao et al., 2024). Therefore, the momentum-learning-rate-based FLMS method tuned by optimization ensures more precise and reliable estimates, making it a preferable option for real-time power frequency applications.

The main contributions of this work are as follows:

- Design of an innovative power frequency estimation scheme considering the momentum-based fractional-order LMS approach.
- Optimization of the co-parameters of the estimator (step size and fractional-order step variables) using the HHO technique. Furthermore, the optimization is improved using chaotic map and opposition-based learning (OBL) methods.
- Verification of the system performance using frequency step changes, frequency ramp changes, and different noise levels. The mean-squared error of the proposed method was also compared with other existing estimation methods.
- Evaluation of estimator robustness by considering signals generated from a hybrid renewable-based power system as well as real time experimental setup.
- Interpretation of the preeminence of the proposed estimator with recently published literature related to the estimated error and rate of convergence.

The remainder of this paper is organized as follows. Section 2 provides a brief description of the momentum-based FLMS algorithm. Section 3 describes the HHO optimizer and its improved version, i.e., chaotic-based HHO with OBL. Section 4 outlines the power system frequency model. Section 5 presents the validation of the estimation scheme by considering various cases. Finally, Section 6 provides some concluding remarks and scope for future work.

2 Momentum-learning-rate-based FLMS algorithm

The FLMS algorithm was originally developed by applying fractional calculus to the conventional LMS algorithm. Here, a fractional-order derivative is used in addition to a simple integer-order derivative to calculate the fractional-order gradient that minimizes the cost function. The fractional order adds a proportionate value of the gradient to the weight updating equation, resulting in better convergence than the standard LMS algorithm.

Let y(k) be the estimated signal and d(k) denote the desired signal; then, the error signal e(k) is represented as d(k)-y(k). The cost function that minimizes the absolute square of the error signal and is represented in Equation 1.

$$J(k) = Min.\ e^2(k) = Min.\ |d(k) - y(k)|^2 \tag{1}$$

The estimated signal is shown in Equation 2, where w represents the weight vector and u is the input signal. The weight vector is crucial for dynamically adjusting the algorithm's coefficients to minimize the estimation error and improve the convergence speed; this ensures that the system adapts effectively to varying signal conditions.

$$y(k) = w(k)\,u(k) \tag{2}$$

Thus, the updated weight equation is calculated by taking the derivative of the cost function with respect to w and is given in Equation 3.

$$\frac{\partial J(k)}{\partial w} = 2e(k)\,\frac{\partial e(k)}{\partial w} \tag{3}$$

Substituting the value of e(k) in Equation 3 and simplifying gives the value which is stated in Equation 4.

$$\frac{\partial J(k)}{\partial w} = -2e(k)\,u(k) \tag{4}$$

The standard LMS algorithm can be formulated by considering Equation 4; the weight updating expression is given by Equation 5, in which the step size (a constant) of the LMS algorithm is μ_1.

$$w(k+1) = w(k) - \frac{1}{2}\mu_1\frac{\partial J(k)}{\partial w} \tag{5}$$

The LMS method in Equation 5 is updated using the first-order gradient. However, the FLMS method takes into account the fractional-order gradient in addition to the first-order gradient. Therefore, Equation 6 is the adaptive weight updating equation for the FLMS approach, where μ_F is the fractional-order gradient step size.

$$w(k+1) = w(k) - \frac{1}{2}\mu_1\frac{\partial J(k)}{\partial w} + \mu_F\frac{\partial^F J(k)}{\partial w^F} \tag{6}$$

Using the Caputo and R-L definition, the fractional derivative D^F of order F of a given function g(t) at the k^{th} instance is described by Equation 7, where the gamma function is represented as $\Gamma(k)$. Specifically, the gamma function is used to generalize the factorial function to non-integer values, which allows the incorporation of fractional powers during the weight update process.

$$D^F g(t) = \frac{\Gamma(k+1) \times t^{k-F}}{\Gamma(k-F+1)} \quad and\ \Gamma(k) = (k-1)! \tag{7}$$

Considering this simplification, the fractional gradient of the FLMS equation is given by

$$\frac{\partial^F J(k)}{\partial w^F} = -2\{e(k)\,u(k)\}\frac{\partial^F w(k)}{\partial w^F} \tag{8}$$

Applying Equation 7 in Equation 8 allows simplification as shown in Equation 9.

$$\frac{\partial^F J(k)}{\partial w^F} = -2\{e(k)\,u(k)\}\left(\frac{\Gamma(2)\,w^{1-F}(k)}{\Gamma(2-F)}\right) \tag{9}$$

Since $\Gamma(2) = 1$, the final recursive weight update equation of the FLMS algorithm after simplification is given in Equation 10.

$$w(k+1) = w(k) + 2\mu_1(e(k)\,u(k)) + \frac{1}{\Gamma(2-F)}\mu_F e(k)\,u(k) \oplus |w|^{1-F}(k) \tag{10}$$

The latter term of Equation 10 summarizes the elementwise multiplication, and the absolute value of the weight vector is considered for preventing trapping of the complex value. The abovementioned term is further improved by incorporating the momentum learning term in the FLMS weight update equation. The momentum term handles the prior gradient and incorporates it into the weights on hand, which speeds up the optimal search and prevents trapping in a local minimum. However, appropriate selection of the momentum learning rate, fractional order, and other constants is necessary to achieve balance between speed and accuracy. Equations 11, 12 describes the revised weight update equation, which is denoted as the imFLMS weight update equation:

$$w(k+1) = w(k) + p(k+1) \tag{11}$$

$$p(k+1) = \gamma p(k) + q(k);\ q(k) = 2\mu_1(e(k)u(k)) + \frac{1}{\Gamma(2-F)}\mu_f e(k)u(k) \oplus |w|^{1-F}(k) \tag{12}$$

where γ is a momentum learning control term in the range of 0–1 that adds a percentage of the previous gradient to the current equation. This update equation is used to estimate the frequency upon optimization, as described in the frequency estimation modeling in Section 4.

The complexities of several algorithms, such as the LMS, FLMS, and imFLMS algorithms, were assessed on the basis of the number of operations needed in the adaptation process (Zubair et al., 2018); these findings are displayed in Table 1. The LMS algorithm necessitates 2M + 1 multiplications and 2M additions in each iteration of the weight adaptation process, where M represents the number of unknown weight parameters. The FLMS approach necessitates 4M + 2 multiplications, 3M additions, and M power calculations, whereas the imFLMS scheme necessitates 5M + 2 multiplications, 4M additions, and M power calculations. The imFLMS method thus requires M additional multiplications and additions over the FLMS approach. Similarly, the FLMS and imFLMS methods require 2 and 2.5 times more multiplications than the LMS approach, respectively. The asymptotic complexity bound for all algorithms is O(M), meaning that the number of operations required increases linearly with the size of the inputs. The fractional order or momentum learning rate in the update equation does not significantly increase the complexity of the proposed algorithm compared to other LMS approaches and its similar versions.

3 Optimization algorithm

3.1 Motivation

Two constants ($\mu_1 and \mu_F$) are associated with the imFLMS algorithm weight update equation and have values between 0 and 1. It is observed from literature that there is no established procedure for selecting the values of these constants. In other words, these constants are assigned values either manually or through the trial and error method, which may impact the system performance parameters such as convergence speed severely. A lot of time is also needed to identify the optimal combination of values that produces an effective outcome. Hence, the selection of constants is achieved with the help of an optimization algorithm in this study. The square of the error signal is considered the cost function, and the optimal value of the constant is set as a constraint described by Equation 13. The upper and lower bounds of both constraints are considered 1 and 0, respectively. Once the optimization is formulated, the optimal values of the constants are searched so that the errors are minimal, as reported below.

$$\begin{aligned} &J(k) = Min.\ e^2(k) = Min.\ |d(k) - e(k)|^2 \\ &Subject\ to:\ 0 < \mu_1 < 1 \\ &0 < \mu_F < 1 \end{aligned} \tag{13}$$

3.2 HHO technique

The HHO belongs to a family of modern metaheuristic algorithms based on the collective hunting behaviors of Harris hawks. Rabbits are the principal food items of Harris hawks and often flee from the hawks (Heidari et al., 2019). As a result, two dynamic factors, namely surprise attack by the hawk and the rabbit's capacity to flee, form the basis for the HHO algorithm. The two steps of the optimizer are exploration and exploitation; there are four substages under exploitation: soft and hard besiege as well as soft and hard besiege with successive fast dives. Figure 1 depicts the methods of exploration and exploitation (Alabool et al., 2021).

3.2.1 Exploration

Harris hawks watch over rabbits from their perches in tall branches. They choose two locate-and-capture strategies with equal chances of success. In the first strategy, the hawk creates a brand-new solution based on a random position, while in the second strategy, another hawk creates a solution based on its present optimal position

TABLE 1 Computational complexities of the proposed algorithm.

Estimation algorithm	Operations			Order of the algorithm
	Multiplication	Addition	Exponentiation	
LMS	2M + 1	2M	0	M
FLMS	4M + 2	3M	M	M
imFLMS	5M + 2	4M	M	M

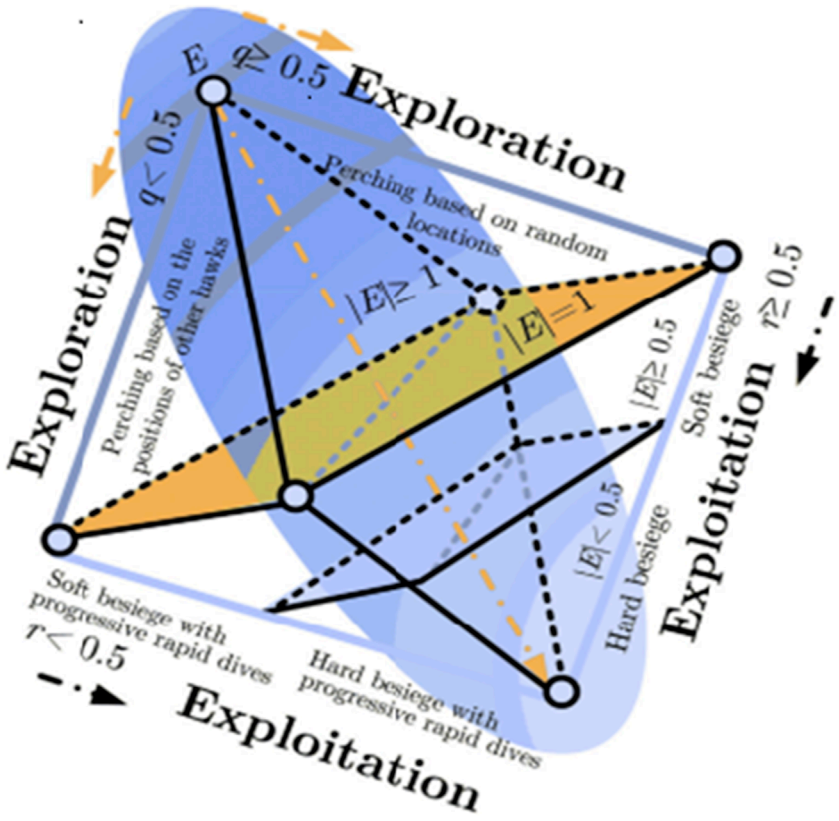

FIGURE 1
Principle of the HHO method (Heidari et al., 2019).

and the mean of each agent. The following mathematical modeling can be considered to mimic such a scenario depicted in Equation 14.

$$X_{t+1} = \begin{cases} X_{rand} - r_1 \left| X_{rand} - 2r_2 X_t \right| & , q_1 \geq 0.5 \\ X_{rabbit} - X_{mean} - r_3 \left(Lb + r_4 \left(Ub - Lb \right) \right), & q_1 < 0.5 \end{cases}, \quad (14)$$

where X_t and X_{rand} are the current and random positions of the hawk, respectively, while X_{t+1} is the next location of the hawk; similarly, X_{mean} is the average of all positions. All the other variables, namely, q, r_1, r_2, r_3, r_4, Lb, and Ub, are generated randomly and have uniform distributions between 0 and 1. An important parameter called "escape energy of the prey" that controls the shift from the exploration to exploitation stages is denoted in Equation 15.

$$E = 2E_0 \left(1 - t/t_{iter} \right), \quad (15)$$

where E is the escape energy, t is the number of iterations currently being performed, and t_{iter} is the maximum number of iterations. E_0 is the starting energy whose value ranges from 0 to 1 for each iteration; accordingly, the escape energy diminishes as the number of iterations increases. When the energy is ($|E| \geq 1$), the corresponding stage is exploration, meaning that the Harris hawks are looking for prey and will explore around their present locations. However, when ($|E| < 1$), the hawks are considered to be attempting to target the prey, indicating the exploitation stage.

3.2.2 Exploitation

Hawks may restrict their prey during this stage, but the animals constantly try to elude the hawks using various methods. Therefore, the optimizer identifies four potential strategies to counteract

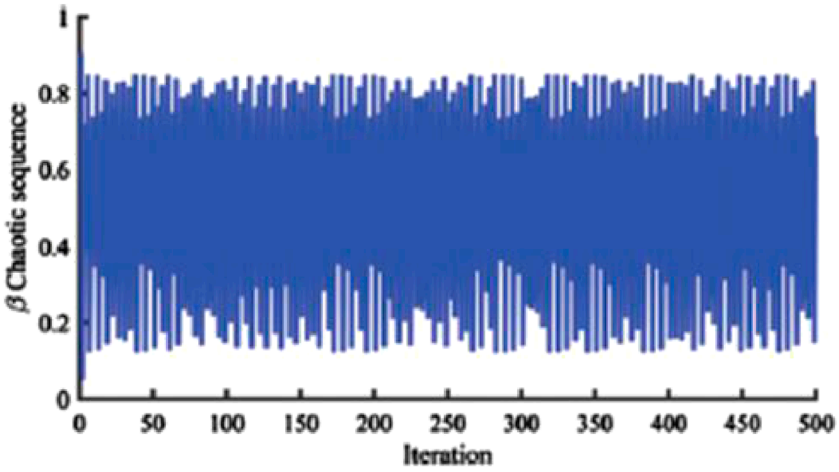

FIGURE 2
β-chaotic function.

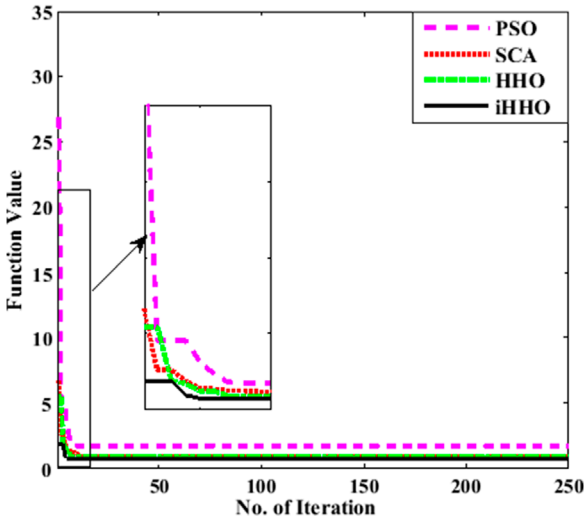

FIGURE 3
Convergence graphs for the proposed and comparison algorithms.

these methods. Let r be the likelihood that a prey will escape an unexpected attack; in this case, if the likelihood is equal to or greater than 0.5, it signifies that the prey can successfully evade attack; conversely, this attempt is deemed unsuccessful if the probability is less than 0.5. However, unless a prey is specifically targeted, hawks always circle their prey. The E value for this situation is used to decide whether to besiege the prey softly or firmly. Thus, $|E| \geq 0.5$ denotes a soft siege while ($|E| < 0.5$) denotes a hard siege.

3.2.2.1 Soft besiege

When both r and $|E|$ are ≥ 0.5, the prey is able to flee from the hawks, but the predator has it surrounded before attacking abruptly; this stage is known as a soft besiege. The mathematical formulation for this method is given by Equation 16, where r_5 is a random number between 0 and 1.

$$X(t+1) = X_{rabbit} - X_t - E\left|\left(2\left(1-r_5\right)X_{rand}\right) - X_t\right| \tag{16}$$

3.2.2.2 Hard besiege

In this stage, $r \geq 0.5$ and $|E| < 0.5$, which is a sign that the prey has a relatively low energy level and that the hawks have it surrounded until the objective is achieved or the prey is captured. Equation 17 presents the mathematical expression for hard besiege.

$$X_{t+1} = X_{rabbit} - E\left|X_{rabbit} - X_t\right| \tag{17}$$

3.2.2.3 Soft besiege with progressive rapid dives

During this stage, $r < 0.5$ and $|E| > 0.5$, suggesting that a more energetic prey can escape from the hawks, at which point the hawks begin to organize a soft siege. Levy-flight function is taken into account in the optimizer to formulate the spontaneous and unpredictable movements of the prey and surprise dives of the hawks. Furthermore, according to several studies, the levy-flight state is one of the best search methods for this and similar foraging situations. The course followed by the hawks thereafter is shown in Equation 18, after which they start diving under the levy-flight condition shown in Equation 19.

$$Y = X_{rabbit} - E\left|2\left(1-r_5\right).X_{rabbit} - X_t\right| \tag{18}$$

$$Z = Y + S \times LV(S) \tag{19}$$

where S is a vector of size 1 × dimension (D), and LV is the levy-flight function represented by Equation 20.

$$LV = \frac{\mu \times \delta}{|v|^{1/\beta}}, \quad \delta = \left(\frac{\Gamma(1+\beta) \times \sin\left(\frac{\Pi\beta}{2}\right)}{\left(\Gamma(1+\beta)/2\right) \times \beta \times 2^{\frac{\beta-1}{2}}} \right)^{1/\beta}. \tag{20}$$

In the above expression, μ, v, and β are all constants equal to 1.5 in this study. Accordingly, the updating expression used at this step

TABLE 2 Performance comparisons for various fractional orders and momentum learning rates.

Technique	Momentum learning rate	Convergence time (ms)				Estimated frequency error (Hz)			
		Fractional order (F)				Fractional order (F)			
		0.2	0.6	0.75	0.9	0.2	0.6	0.75	0.9
imFLMS	0.2	1.258	1.086	0.954	0.955	0.0006	0.0017	0.0046	0.0074
	0.5	1.027	0.960	0.908	0.895	0.0003	0.0021	0.0058	0.0087
	0.7	0.851	0.869	0.804	0.801	0.0002	0.0018	0.0079	0.0092
	0.9	0.847	0.846	0.720	0.698	0.0003	0.0048	0.0157	0.0350
mFLMS	0.2	1.155	1.089	0.954	0.955	0.0006	0.0021	0.0048	0.0074
	0.5	1.035	0.840	0.908	0.866	0.0003	0.0021	0.0058	0.0092
	0.75	0.821	0.701	0.804	0.824	0.0002	0.0019	0.0067	0.0099
	0.9	0.822	0.864	0.790	0.798	0.0003	0.0081	0.0277	0.0411
LMS	-	2.331				0.0181			

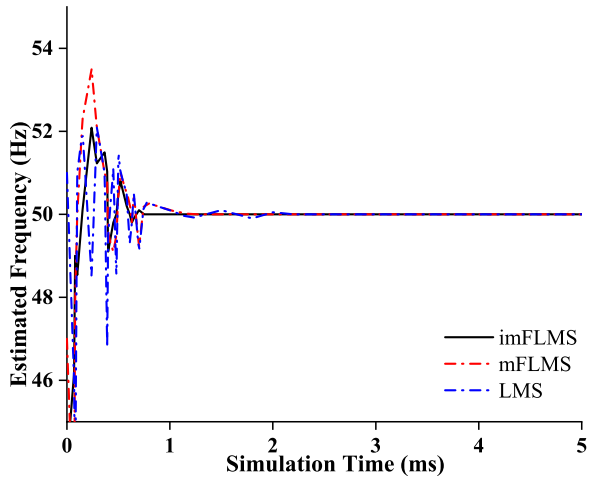

FIGURE 4
Comparison of frequencies estimated by various techniques.

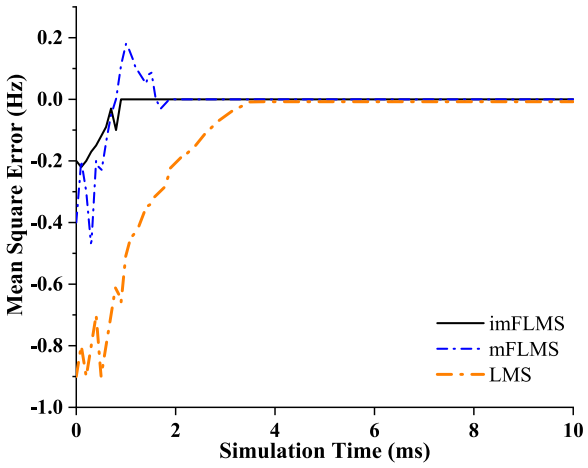

FIGURE 5
Comparison of the mean-squared errors for frequencies estimated by various methods.

is based on a comparison of the current location with the previous value that represented in Equation 21.

$$X(t+1) = \begin{cases} Y & : if F(Y) < F(X) \\ Z & : if F(Z) < F(X) \end{cases}. \quad (21)$$

3.2.2.4 Hard besiege with progressive rapid dives

Under this condition, $|E| < 0.5$ and $r < 0.5$, indicating that the hawks must continue a hard siege on the prey while it lacks the energy to flee. Another method of categorizing this situation is that the prey is under gentle besiege while the hawks maintain their hard pace, working to close the average distance between. Equation 22 is used to mathematically describe the fitness values of Y' and Z'.

$$X(t+1) = \begin{cases} Y' & : if F(Y') < F(X) \\ Z' & : if F(Z') < F(X) \end{cases} \quad (22)$$

Then, Y' and Z' are obtained using Equations 23, 24, respectively.

$$Y' = X_{rabbit} - E\left|\{2(1-r_5).X_{rabbit}\} - X_m\right| \quad (23)$$

$$Z' = Y' + S \times LV(S) \quad (24)$$

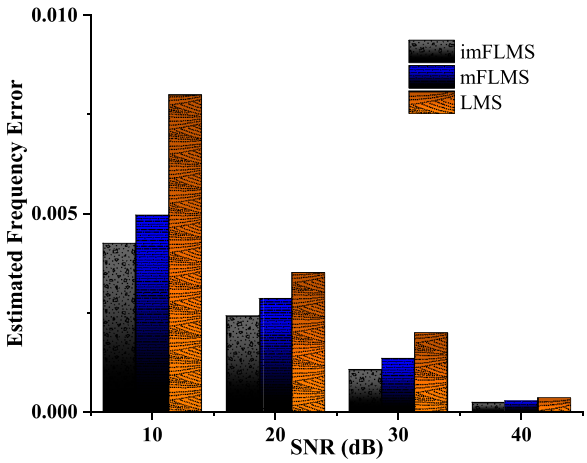

FIGURE 6
Bar chart representing the signal-to-noise ratio (SNR) vs. error for different methods.

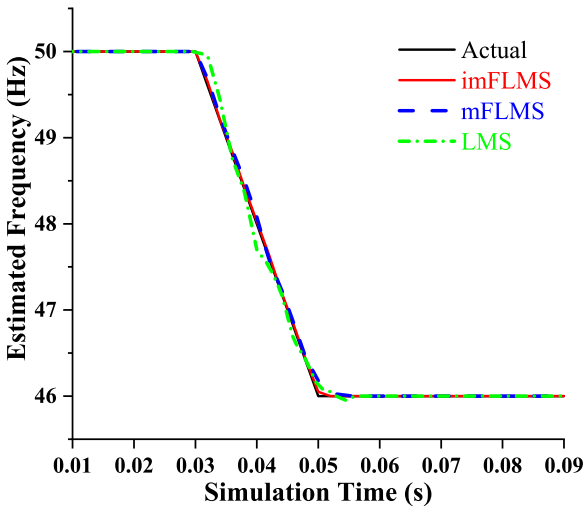

FIGURE 8
Frequency estimations with a ramp change.

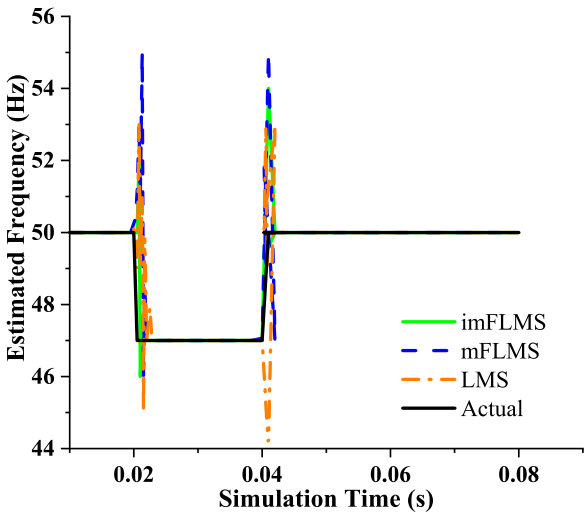

FIGURE 7
Frequency estimations with a step change.

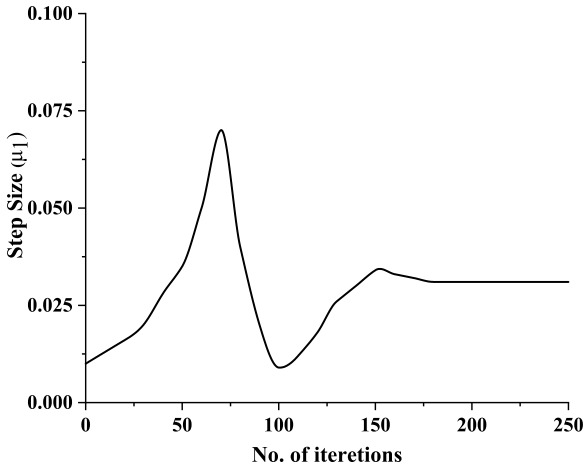

FIGURE 9
Variation of the step size parameter with the iHHO approach.

3.3 Motivation for the improved HHO algorithm based on OBL and iHHO

Most of the metaheuristic algorithms start with a random variable for initialization and corresponding distribution. Recently, chaotic mapping has been used in such metaheuristic techniques as it allows similar properties and characteristics as randomness, with improved dynamic and statistical performances. Therefore, chaotic mapping is added to the unique swarm intelligence approach in place of a random variable. As added advantages to the optimization strategy, this mapping offers accurate initialization, arbitrariness, and ergodicity (Baliarsingh and Vipsita, 2020). By producing non-repeated numbers with periodicity, chaotic mapping enhances the efficiency with respect to a random number. These characteristics resulting from chaotic mapping provide the means to escape local optima and preserve distinction while increasing the efficacy of the global search. Appropriate initialization is achieved when the preliminary points are adjusted such that a meaningful result is generated, assuming that the outcome is wisely dependent on the preliminary points. Throughout the phase of arbitrariness, chaotic mapping takes on the roles of the random variables. Ergodicity describes the capacity of a chaotic variable to identify non-repeated values given a specific range.

Different metaheuristic methods have been used to implement various chaotic functions. Recently, Zahmoul et al. (2017) reported a new approach to the family of chaotic functions; Equation 25

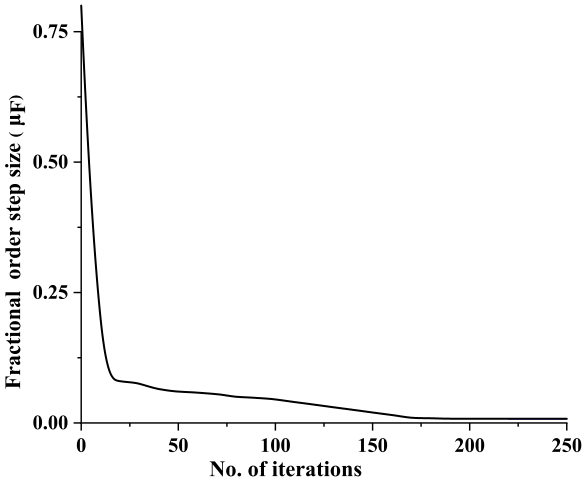

FIGURE 10
Variation of the fractional-order step size parameter with the iHHO approach.

provides the mathematical representation of this mapping:

$$\beta(x{:}p,q,x_1,x_2) = \begin{cases} \left(\frac{x-x_1}{x_c-x_1}\right)^p \left(\frac{x_2-x}{x_2-x_c}\right)^q & ,if\, x \in x_1,x_2 \\ 0 & ,\quad otherwise \end{cases}, \tag{25}$$

where $x_1, x_2, p, q \in R$ *and* $x_1 > x_2$ are calculated using the following Equations 26–29.

$$x_c = \frac{px_1 + qx_2}{p+q} \tag{26}$$

$$p = a_{11} + b_{11}c \tag{27}$$

$$q = a_{22} + b_{22}c \tag{28}$$

$$X_{t+1} = k\beta(x_t{:}p,q,x_1,x_2) \tag{29}$$

where c is the bifurcation parameter; a_{11}, a_{22}, b_{11}, and b_{22} are constants. The β-chaotic map exhibits initialization and variation sensitivity, and its bifurcation diagram is shown in Figure 2. The bifurcation diagram is often used to demonstrate the values that approach asymptoticity to a given system state as a function of the bifurcation parameter, where the abscissa represents the bifurcation parameter and ordinate indicates the range of values of the map that approaches asymptoticity subject to the initial conditions.

Exploration and exploitation are appropriately balanced when chaotic mapping is applied to the traditional HHO algorithm. Chaotic mapping replaces the random functions employed in traditional HHO techniques. Then, the constants q, r_1, r_2, r_3, r_4, Lb, and Ub (from Equation 14) are all considered to be 0 if $x_t > 0.5$ or 1 if $x_t < 0.5$, where x_t is the chaotic mapping of the t_{th} iteration.

A fresh and practical theory for improving the performances of diverse metaheuristic approaches from an optimization standpoint is OBL. The idea of OBL is to take the opposite candidate as an alternative approach to reach the optimal solution, which could be closer to the global optimum solution. The objective of OBL in optimization is to improve the solution's effectiveness by evaluating the contender for the solution of the relevant pair. The ideal response candidate is taken into account for the subsequent individual solution (Barisal and Prusty, 2015). Suppose that Z_i denotes the candidate solution; then, its corresponding opposite candidate solution Z_i' can be calculated as per Equation 30, where L and U represent the lower and upper bounds of the search space of the constraints, which are 0 and 1 in our case, respectively.

$$Z_i' = L + U - Z_i \tag{30}$$

The global searchability is enhanced with OBL, and the solution using this method with chaotic mapping is shown in Equation 31. In this instance, Z_{min} and Z_{max} are the lower and upper bounds, respectively, while Z'_{hho} is the opposing candidate hawk; Z_{hho} displays the hawk's position vector, while Z_{best} displays the hawk's optimal solution; x_t denotes the chaotic mapping.

$$Z'_{hho} = Z_{\max} + Z_{\min} - Z_{best} + x_t\left(Z_{best} + Z_{hho}\right) \tag{31}$$

4 Frequency estimation modeling

The instantaneous voltage signals of the three phases of a power system can be expressed as follows:

$$\begin{aligned} v_{an} &= V_{an}\sin\left(\omega_o n\Delta T_s + \Phi\right) + \eta_a \\ v_{bn} &= V_{bn}\sin\left(\omega_o n\Delta T_s + \Phi - \frac{2\pi}{3}\right) + \eta_b \\ v_{cn} &= V_{cn}\sin\left(\omega_o n\Delta T_s + \Phi + \frac{2\pi}{3}\right) + \eta_c \end{aligned} \tag{32}$$

where the peak values of the three-phase voltage signals at the time instant n are denoted by the variables v_{an}, v_{bn}, and v_{cn}; $\Delta T_s = 1/f_s$ is the sample interval, with f_s being the sampling frequency; ϕ represents the phase angle at the beginning of the measurement; $\omega_o = 2\pi f_s$ is the angular frequency of the voltage signal, where f_0 is the fundamental frequency of the system; η_a, η_b, and η_c are the additive white Gaussian noise (AWGN) components present in the individual phases.

Applying Clarke's transform to the three-phase voltage signals in Equation 32 results in the complex-valued power system voltage signal (also known as the $\alpha\beta$ signal) shown in Equation 33.

$$\begin{bmatrix} V_{\alpha d} \\ V_{\beta d} \end{bmatrix} = \sqrt{2/3}\begin{bmatrix} 1 & -1/2 & -1/2 \\ 0 & \sqrt{3}/2 & -\sqrt{3}/2 \end{bmatrix}\begin{bmatrix} V_{an} & V_{bn} & V_{cn} \end{bmatrix}^T \tag{33}$$

In the complex-valued voltage signal, $V_{\alpha d}$ and $V_{\beta d}$ denote the real and imaginary parts, respectively. Since the measured complex signal produced by the components is tainted by AWGN, it can be written as Equation 34.

$$d(k) = V_{\alpha d} + jV_{\beta d} + \eta_d = Ae^{j\omega_o\Delta T_s + \eta_d} \tag{34}$$

In the above expression, $d(k)$ represents the desired three-phase voltage signal. Similarly, the estimated voltage signal $y(k)$ is formulated through state-space modeling as shown in Equation 35 where u is the input vector equal to [0 1] and w is the weight

TABLE 3 Frequency estimation errors for different techniques.

Technique	Frequency estimation error (Hz)				Execution time (ms)
	10 dB	20 dB	30 dB	40 dB	
imFLMS	0.4251	0.0242	0.0074	0.0051	0.541
mFLMS	0.4960	0.0286	0.0085	0.0072	0.484
LMS	0.7991	0.0351	0.0015	0.0019	0.408

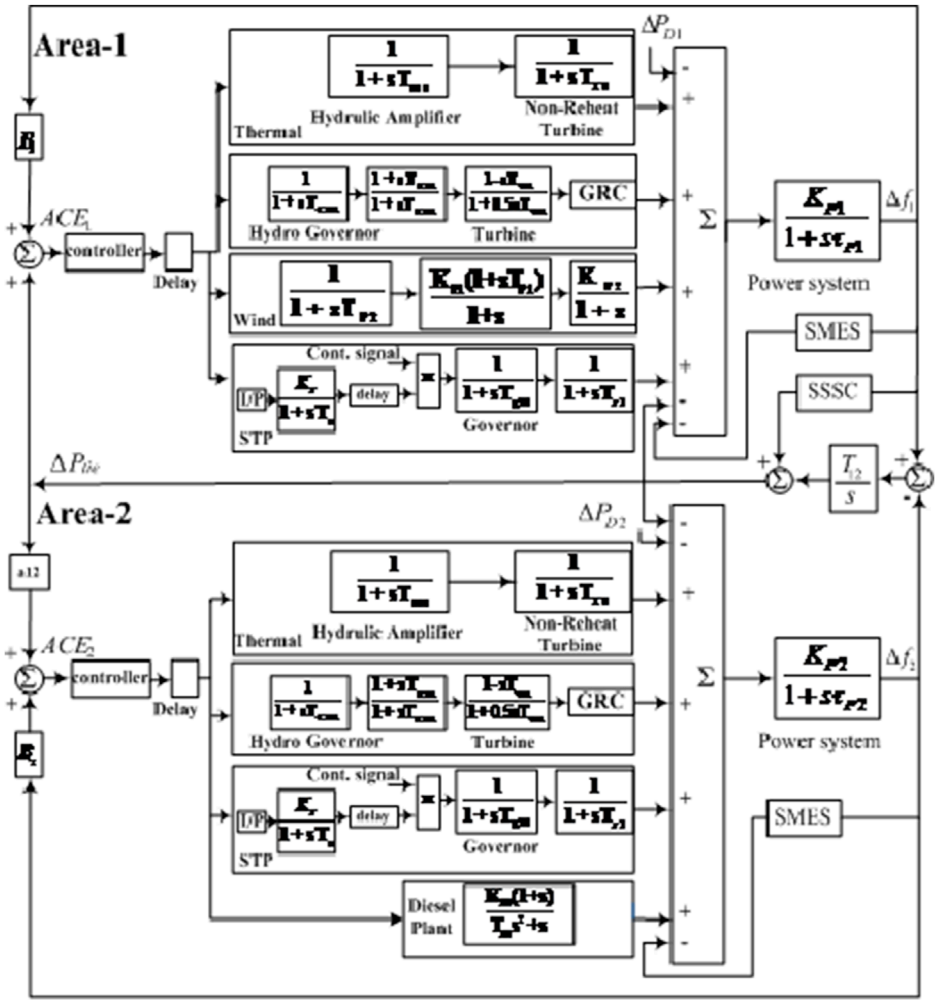

FIGURE 11
Test system under consideration.

vector given by $[w_k(1)\ w_k(2)]$, where $w_k(1) = e^{j\omega_o \Delta T_s}$ and $w_k(2) = Ae^{j\omega_o k\Delta T_s + \eta_d}$.

$$y(k) = w \times u^T. \tag{35}$$

The input vector is updated by following the imLMS weight updating equation as stated in Equations 11, 12. Therefore the observed voltage signal and error [e(k) = d(k)-y(k)] is also updated in each Kth iteration. In the process, iHHO optimizer is also introduced in the weight updating equation. Thus, the process becomes effective and efficient. When the mean square error approximates to zero, the optimizer provides the optimal step sizes which automatically fetch to the weight updating equation and the system power frequency will be estimated using Equation 36.

$$\widehat{f}_n = \mathrm{Im}g\left(\log w_k(2)/2\pi T_s\right). \tag{36}$$

The general steps involved in the proposed estimator are as follows:

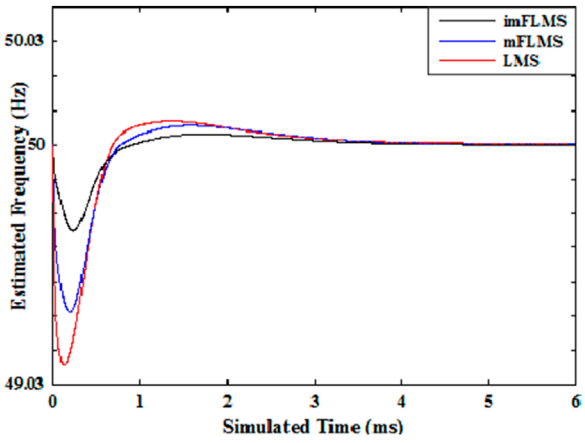

FIGURE 12
Estimated frequencies of the test system based on different methods.

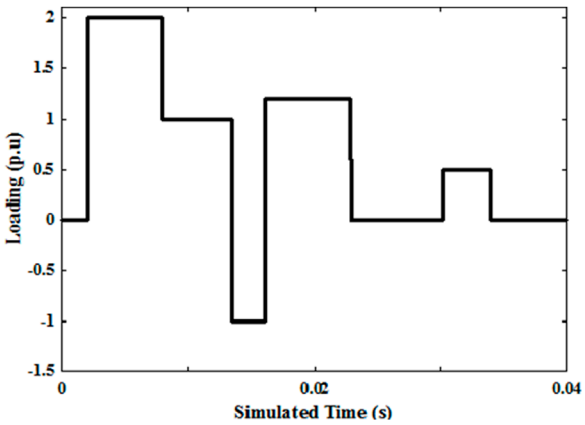

FIGURE 13
Random load signal applied to the test system.

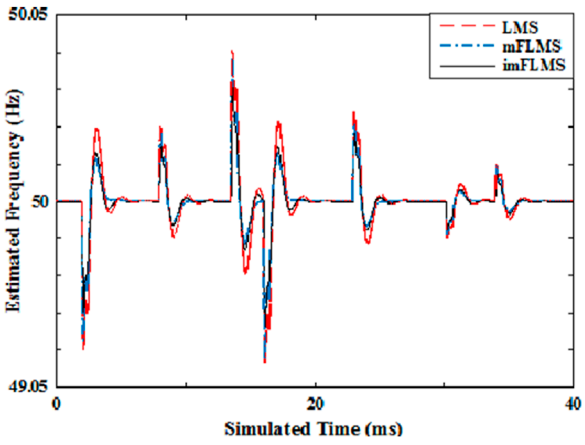

FIGURE 14
Frequencies estimated by different methods for random loading.

Step (1). Initialization of the input vector, weight vector, and all variables.
Step (2). Formulation of the instantaneous voltage signal using Equation 32.
Step (3). Decomposition of voltage signal into its complex form using Equation 33.
Step (4). Conceptualization of the observed voltage signal through Equation 35.
Step (5). Updating the weight vector using the imFLMS estimator as per Equation 11.
Step (6). Optimal tuning of the step size and fractional-order step size with the optimization algorithm.
Step (7). Calculation of the frequency component from the weight update equation using Equation 36.

5 Summary of results and discussion

5.1 Validation of the proposed improved HHO algorithm

The improved HHO algorithm was used to obtain the optimal step size that minimizes the cost function of the proposed imFLMS estimation algorithm. Several distinct benchmark functions were used to verify the reliability and effectiveness of the proposed technique. The improved HHO showed greater optimal performance after 100 trials. The enhanced version is more accurate and resilient while requiring less processing time; the ideal solution demonstrates higher search process efficiency and flawless balance between exploration and exploitation while handling the benchmark functions. Figure 3 shows the convergence graph for comparison, where the optimization approach offers a more optimal value than the traditional HHO, SCA, and PSO techniques. The graphs show that the suggested iHHO algorithm maintains its ideal outcome in terms of fewer iterations and shorter execution time. The proposed optimizer was also applied to several common restricted benchmark functions, such as Mishra's bird, Simionescu, and Townsend functions, as well as unconstrained benchmark functions like the Ackley, Levi, and Rastrigin functions (Pati and Subudhi, 2023). Their results show that the iHHO algorithm outperforms the other algorithms in terms of the best, worst, and mean values as well as execution time.

5.2 Temporal complexity of the proposed optimization algorithm

The temporal complexity of the proposed algorithm can be computed as follows and stated in Equation 37.

- Time required for population initialization.
- Time needed to estimate each particle's fitness value.

Thus, the algorithm performs

$$O(L + U + D_m + Max_{iter}) \tag{37}$$

where O() represents the order; D_m is the problem size; L and U are the lower and upper bounds, respectively; Max_{iter} is

FIGURE 15
Experimental setup for real-time data generation.

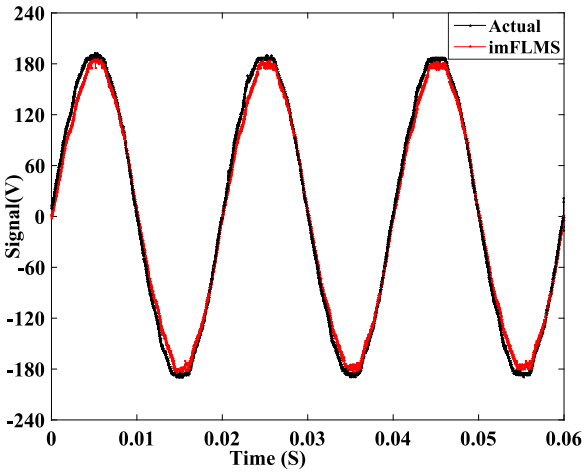

FIGURE 16
Actual waveform and estimated signal using the proposed method with the experimental setup.

the maximum number of iterations. The execution times based on the suggested technique for different estimation algorithms are presented in Tables 2, 3.

5.3 Frequency estimation from three-phase balanced signals

Using filtering methods based on the LMS, mFLMS, and the newly proposed imFLMS algorithms, several examples of balanced power signals were simulated as follows.

The control parameters of the weight update expression (μ_1 and μ_F) were tuned using the improved HHO technique, and the remaining variables like the momentum learning term and fractional order were assigned based on system performance. The values of all constants and variables were evaluated using MATLAB/Simulink. For the purpose of the simulations, the voltage equations for a balanced three-phase system were considered according to Equation 32; the phase signal amplitudes V_{an}, V_{bn}, and V_{cn} were each considered to be 1 p.u. in this study. The signal frequency was considered to be 50 Hz, and AWGN with a signal-to-noise ratio (SNR) of 30 dB was introduced to corrupt the complex phasor produced by the transform. The comparisons were performed to determine whether the proposed adaptive filtering technique provides the most accurate estimation. The frequency estimation plot of the proposed technique was compared with those of the mFLMS and standard LMS techniques, and it was observed that the proposed method estimated the frequency well before the other techniques, as displayed in Figure 4. A comparison of the mean-squared errors of the various frequency estimation techniques is depicted in Figure 5; here, the imFLMS method was observed to have faster error convergence over the other adaptive algorithms. The absolute frequency inaccuracy was found by determining the difference between the desired value and estimated output from the adaptive algorithm. A comparative assessment of the estimated errors for different SNRs is further shown in the bar chart of Figure 6. Although the imFLMS, mFLMS, and LMS algorithms can provide frequency estimations, their effectiveness reduces in noisier environments.

The power system signal with a fundamental frequency of 50 Hz was then applied with a step shift in frequency between 0.02 and 0.04 s, for which it was observed that the imFLMS estimation technique followed the frequency variation more closely than the other algorithms (Figure 7). Next, a ramp shift in frequency from 50 Hz to 46 Hz was applied between 0.03 and 0.05 s, following which the frequency was maintained constant at 46 Hz for the remainder of the period of the three-phase signal. As seen in Figure 8, the suggested technique successfully tracks the signal ramp change with a convergence time of less than half a cycle and a high degree of estimation accuracy. With the FLMS algorithm, the tracking began at about 0.033 s and leading to an inconsistent result. Similarly, as seen in the figure, the LMS algorithm followed the ramp variation from 0.038 s.

The step size variation μ_1 with respect to number of iterations for the proposed iHHO algorithm is displayed in Figure 9. Here, the adaptive algorithm approach suggests that the optimal step size selection should satisfy the condition of 0 < step size < 1/(maximum eigenvalue of the input autocorrection matrix). Thus, the highest allowed value is obtained initially, and the step size is reduced thereafter until the change in error is

TABLE 4 Comparative assessment with the state-of-the-art methods.

Method	Convergence rate		Estimated error	
	Reported (ms)	Amelioration (%)	Reported	Amelioration (%)
Proposed imFLMS	0.8	-	0.007	-
Sparse H_{∞} filter (Subudhi et al., 2020)	1.2	150	0.008	114.28
Linear LMS kurtosis (Nefabas et al., 2020)	3	375	0.009	128.57

stabilized. A similar behavior was also observed with the proposed model. However, the main feature here is that the selection process automatically addresses the aforementioned condition. The improved optimization is so effective that the optimal value (0.031) is identified well before the 200th iteration. Similarly, the fractional-order step size variation based on the iterations of the optimizer algorithm is shown in Figure 10 and is found to be 0.0012.

Table 2 displays the performance evaluation results for the suggested scheme in terms of the initial convergence rates for different momentum learning rates (γ) and fractional orders (F). The findings reveal that the initial convergence of the imFLMS algorithm is much faster than those of typical adaptive approaches and that the convergence rate increases with increases in the preceding gradients. Estimated frequency error validation was then used to examine the performance of the suggested method further; the results of the imFLMS approach were compared with those of the other methods for various values of γ and F. It is noted that all techniques were sufficiently accurate and convergent; however, the accuracy of any approach decreases as the noise variance increases. It was also found that fractional adaptive algorithms, such as the imFLMS and mFLMS methods, were steady for all possible fractional order variations and that there were no significant variations in accuracy between various fractional orders. Additionally, a larger fractional order value (F = 0.75) produced a considerably better outcome. According to the findings presented in Table 2, the imFLMS algorithm achieves faster convergence when the proportion of prior gradients is relatively high (γ = 0.9) but better steady-state results when this proportion is lower (γ = 0.2). Therefore, a larger value of the learning parameter (γ = 0.7) would be an excellent choice for achieving good balance between faster convergence and better steady-state results. Table 3 shows the performances of the imFLMS, mFLMS, and LMS estimators for various noise levels. As discussed earlier, the proposed imFLMS technique has higher efficacy in noisy environments than other estimation techniques, but its execution time is slight higher than that of the traditional LMS algorithm at different noise levels.

5.4 Frequency estimation with a renewable-based power system

To examine the effectiveness of the proposed scheme, it was tested with a signal derived from a renewable-based two-area-load frequency control model. This power system was earlier modeled and simulated in MATLAB as well as evaluated by Pati and Subudhi (2021). Figure 11 shows the block diagram model of the test system under consideration (Pati and Subudhi, 2021).

To validate the proposed scheme, a signal generated with a step load perturbation of 2% was considered and compared for the suggested imFLMS and existing estimation techniques. Figure 12 displays the relevant comparative plots for these estimation methods. Furthermore, the dynamic load signal shown in Figure 13 was applied to the test system to verify the algorithmic efficacy. The imFLMS, mFLMS, and LMS algorithms were used to estimate the test system frequency, and their results are shown in Figure 14. As verified earlier, the imFLMS algorithm outperforms the other estimation techniques; it estimates the frequency more precisely in less time than the other methods even with the random load, thus proving its robustness.

5.5 Experimental studies and results

To validate the performance of the proposed algorithm for power system frequency estimation, a simple experimental setup was established in the laboratory. In this setup, an induction motor was connected as a load to a single-phase power supply, as suggested by Daw (2016). A variable AC supply was then employed to regulate the input voltage. A voltmeter, an ammeter, and a wattmeter were used to measure the output voltage, current, and power, respectively. The voltage signals were captured using a digital storage oscilloscope from the load side, where the induction motor was connected, as illustrated in Figure 15. The detailed specifications of the equipment used are as follows:

- Variable AC supply: 0–230 V/0–270 V, 10 A
- Voltmeter: 0–150/300 V
- Ammeter: 0–5/10 A
- Wattmeter: 0–150/300 V, 5/10 A
- Single-phase squirrel-cage-type induction motor: power = 1.5 HP, voltage = 230 V, current = 6 A, frequency = 50 Hz, speed = 1440 rpm
- Digital storage oscilloscope: bandwidth = 200 MHz, number of channels = 2, sampling rate = 1 gigasamples/s, probe-PP510 = 100 MHz
- Computer: 2.4 GHz, 8 GB RAM

The input voltage waveform across the induction motor was recorded with a digital storage oscilloscope, and the data were subsequently transferred to a computer through communication software. Figure 16 illustrates the voltage signal estimation using

the proposed imFLMS algorithm and the data obtained from the experiment. The results demonstrate that the proposed algorithm yields an estimation significantly closer to the actual signal and with a nearly identical period. Consequently, the fundamental frequency of 50 Hz was accurately estimated with minimal mean-squared error of 0.0741 Hz, indicating that the proposed estimator was highly effective for applications involving real-world data.

5.6 Comparative assessment with state-of-the-art methods

The percentage improvement was measured in the comparative state-of-the-art study using Equations 38, 39, where AP_1 and AP_2 stand for "amelioration (in percentage)" and represent the percentage enhancements obtained as the performance measures (namely convergence rate and estimated error) compared to the reference schemes noted in Subudhi et al. (2020) and Nefabas et al. (2020). The convergence rate and estimated error have their own amelioration values and are denoted by the notations APi(Convergence) and APi(Error), respectively.

$$AP_1(\%)(Convergence) = \frac{Rate\ of\ Convergence_{\mathrm{Ref}}}{Rate\ of\ Convergence_{Estimated}} \times 100 \quad (38)$$

$$AP_2(\%)(Error) = \frac{Estimated\ Error_{\mathrm{Ref}}}{Estimated\ Error_{obtained}} \times 100 \quad (39)$$

The results for the suggested adaptive scheme tuned by iHHO for power system frequency estimation were compared with those reported by Subudhi et al. (2020) and Nefabas et al. (2020). These comparisons are summarized in Table 4. Additionally, it has been demonstrated beyond reasonable doubt that the proposed method greatly enhances the reaction time of the system. Thus, we conclude that the suggested system configuration has better stability compared to those discussed in Subudhi et al. (2020) and Nefabas et al. (2020). From AP_1 and AP_2, it is observed that the system responsiveness is greatly improved with the iHHO algorithm and proposed technique. The adoption of the imFLMS algorithm results in a convergence rate improvement of 150%–375% and estimated error improvement of 114.28%–128.57% compared to the findings reported by Subudhi et al. (2020) and Nefabas et al. (2020). The sparse H-infinity filtering approach was reported to produce absolute frequency errors of 0.031, 0.008, and 0.0010 at SNR levels of 20 dB, 30 dB, and 40 dB, respectively. In contrast, the proposed imFLMS estimation technique demonstrates superior accuracy at these SNR levels, as detailed in Table 3. Similarly, the linear LMS kurtosis estimator was reported to provide approximate frequency biases of 0.196, 0.0075, and 0.0038 Hz at SNR levels of 20 dB, 30 dB, and 40 dB, respectively.

6 Conclusion

This study presents a novel innovative momentum-learning-control-rate-based fractional-order LMS algorithm for instantaneous frequency estimation that was optimized using improved chaotic-based HHO. The proposed technique is suitable for measuring a wide range of frequency variations and exhibits superior behavior under dynamic conditions. The proposed algorithm was also investigated for step and ramp changes of the frequency signal with different noise levels. Thus, it was found to be a valuable and efficient tool for successful power frequency estimation, with the simulation results confirming the superior dynamic responses of the algorithm. The proposed estimation method with the chaotic and OBL with HHO shows better performance than the approach based on the simple LMS method for waveforms with noise. In addition, this approach is important for real-time signals from test systems. The investigations also verified the efficacy and improved performance of the suggested approach through comparisons with signals derived from a multiarea renewable-based power system model and real time experimental setup. The proposed algorithm is thus expected to be useful for system identification, noise cancellation, and real-time applications.

Data availability statement

The original contributions presented in the study are included in the article/Supplementary Material, and any further inquiries may be directed to the corresponding author.

Author contributions

SP: conceptualization, data curation, formal analysis, funding acquisition, investigation, methodology, project administration, resources, software, validation, visualization, writing–original draft, and writing–review and editing. US: conceptualization, formal analysis, funding acquisition, investigation, methodology, supervision, validation, writing–original draft, and writing–review and editing.

Funding

The authors declare that no financial support was received for the research, authorship, and/or publication of this article.

Conflict of interest

The authors declare that the research was conducted in the absence of any commercial or financial relationships that could be construed as a potential conflict of interest.

Publisher's note

References

Alabool, H. M., Alarabiat, D., Abualigah, L., and Heidari, A. A. (2021). Harris hawks optimization: a comprehensive review of recent variants and applications. *Neural Comput. Appl.* 33, 8939–8980. doi:10.1007/s00521-021-05720-5

Alhelou, H. H., Hamedani-Golshan, M. E., Njenda, T. C., and Siano, P. (2019). A survey on power system blackout and cascading events: research motivations and challenges. *Energies* 12, 682. doi:10.3390/en12040682

Alhussan, A. A., Farhan, A. K., Abdelhamid, A. A., El-Kenawy, E.-S. M., Ibrahim, A., and Khafaga, D. S. (2023). Optimized ensemble model for wind power forecasting using hybrid whale and dipper-throated optimization algorithms. *Front. Energy Res.* 11, 1174910. doi:10.3389/fenrg.2023.1174910

Aslam, M. S., Chaudhary, N. I., and Raja, M. A. Z. (2017). A sliding-window approximation-based fractional adaptive strategy for hammerstein nonlinear armax systems. *Nonlinear Dyn.* 87, 519–533. doi:10.1007/s11071-016-3058-9

Avalos, O., Cuevas, E., Becerra, H. G., Gálvez, J., Hinojosa, S., and Zaldívar, D. (2021). Kernel recursive least square approach for power system harmonic estimation. *Electr. Power Components Syst.* 48, 1–16. doi:10.1080/15325008.2021.1908457

Baliarsingh, S. K., and Vipsita, S. (2020). Chaotic emperor penguin optimised extreme learning machine for microarray cancer classification. *IET Syst. Biol.* 14, 85–95. doi:10.1049/iet-syb.2019.0028

Barisal, A. K., and Prusty, R. (2015). Large scale economic dispatch of power systems using oppositional invasive weed optimization. *Appl. Soft Comput.* 29, 122–137. doi:10.1016/j.asoc.2014.12.014

Bershad, N. J., Wen, F., and So, H. C. (2017). Comments on "fractional lms algorithm". *Signal Process.* 133, 219–226. doi:10.1016/j.sigpro.2016.11.009

Bose, B. K. (2020). Power electronics and motor drives: advances and trends.

Chao, X., Xinze, X., Xin, H., and Can, D. (2024). Parameter identification method of load modeling based on improved dung beetle optimizer algorithm. *Front. Energy Res.* 12, 1415796. doi:10.3389/fenrg.2024.1415796

Chaudhary, N. I., Raja, M. A. Z., He, Y., Khan, Z. A., and Machado, J. T. (2021). Design of multi innovation fractional lms algorithm for parameter estimation of input nonlinear control autoregressive systems. *Appl. Math. Model.* 93, 412–425. doi:10.1016/j.apm.2020.12.035

Chaudhary, N. I., Raja, M. A. Z., and Rehman Khan, A. U. (2015). Design of modified fractional adaptive strategies for hammerstein nonlinear control autoregressive systems. *Nonlinear Dyn.* 82, 1811–1830. doi:10.1007/s11071-015-2279-7

Cheng, S., Wei, Y., Chen, Y., Li, Y., and Wang, Y. (2017). An innovative fractional order lms based on variable initial value and gradient order. *Signal Process.* 133, 260–269. doi:10.1016/j.sigpro.2016.11.026

Daw, N. A. (2016). "Comparison of lab work and simulation results for speed control of single phase induction motor capacitor starting," in *2016 17th international conference on sciences and techniques of automatic control and computer engineering (STA)* (IEEE), 397–402.

Friedman, V. (1994). A zero crossing algorithm for the estimation of the frequency of a single sinusoid in white noise. *IEEE Trans. Signal Process.* 42, 1565–1569. doi:10.1109/78.286978

Han, Y., Luo, M., Zhao, X., Guerrero, J. M., and Xu, L. (2015). Comparative performance evaluation of orthogonal-signal-generators-based single-phase pll algorithms—a survey. *IEEE Trans. Power Electron.* 31, 3932–3944. doi:10.1109/tpel.2015.2466631

Heidari, A. A., Mirjalili, S., Faris, H., Aljarah, I., Mafarja, M., and Chen, H. (2019). Harris hawks optimization: algorithm and applications. *Future gener. Comput. Syst.* 97, 849–872. doi:10.1016/j.future.2019.02.028

Kanoongo, S., and Giri, R. K. (2023). Link quality improvement analysis of relay-assisted hybrid rf/fso systems in challenging environments. *Optik* 294, 171442. doi:10.1016/j.ijleo.2023.171442

Li, J., Teng, Z., Wang, Y., You, S., Liu, Y., and Yao, W. (2019). A fast power grid frequency estimation approach using frequency-shift filtering. *IEEE Trans. Power Syst.* 34, 2461–2464. doi:10.1109/tpwrs.2019.2892599

Man, J., Chen, L., Terzija, V., and Xie, X. (2021). Mitigating high-frequency resonance in mmc-hvdc systems using adaptive notch filters. *IEEE Trans. Power Syst.* 37, 2086–2096. doi:10.1109/tpwrs.2021.3116277

Martinek, R., Rzidky, J., Jaros, R., Bilik, P., and Ladrova, M. (2019). Least mean squares and recursive least squares algorithms for total harmonic distortion reduction using shunt active power filter control. *Energies* 12, 1545. doi:10.3390/en12081545

Menesy, A. S., Sultan, H. M., Selim, A., Ashmawy, M. G., and Kamel, S. (2019). Developing and applying chaotic harris hawks optimization technique for extracting parameters of several proton exchange membrane fuel cell stacks. *IEEE Access* 8, 1146–1159. doi:10.1109/ACCESS.2019.2961811

Mojiri, M., Karimi-Ghartemani, M., and Bakhshai, A. (2007). Estimation of power system frequency using an adaptive notch filter. *IEEE Trans. Instrum. Meas.* 56, 2470–2477. doi:10.1109/tim.2007.908631

Naik, P. A., Zehra, A., Farman, M., Shehzad, A., Shahzeen, S., and Huang, Z. (2024). Forecasting and dynamical modeling of reversible enzymatic reactions with a hybrid proportional fractional derivative. *Front. Phys.* 11, 1307307. doi:10.3389/fphy.2023.1307307

Nefabas, G. L., Zhao, H., and Xia, Y. (2020). Widely linear least mean kurtosis-based frequency estimation of three-phase power system. *IET Generation, Transm. and Distribution* 14, 1159–1167. doi:10.1049/iet-gtd.2018.6498

Pan, X., Zhang, L., and Huang, H. (2021). Harmonic cancellation by adaptive notch filter based on discrete wavelet packet transform for an mmcc-statcom. *IEEE Trans. Power Deliv.* 37, 1834–1844. doi:10.1109/tpwrd.2021.3099201

Pati, S. S., and Subudhi, U. (2021). "Frequency regulation of solar-wind integrated multi-area system with smes and sssc," in *2021 IEEE international power and renewable energy conference (IPRECON)* (IEEE), 1–4.

Pati, S. S., and Subudhi, U. (2023). Stability analysis of a multi-area renewable system and frequency control with improved chaotic harris hawk optimization algorithm. *Arabian J. Sci. Eng.* 49, 6531–6550. doi:10.1007/s13369-023-08313-7

Sharma, R., Sethares, W. A., and Bucklew, J. A. (1998). Analysis of momentum adaptive filtering algorithms. *IEEE Trans. Signal Process.* 46, 1430–1434. doi:10.1109/78.668805

Shehab, M., Mashal, I., Momani, Z., Shambour, M. K. Y., AL-Badareen, A., Al-Dabet, S., et al. (2022). Harris hawks optimization algorithm: variants and applications. *Archives Comput. Methods Eng.* 29, 5579–5603. doi:10.1007/s11831-022-09780-1

Subudhi, U., Sahoo, H. K., and Mishra, S. K. (2020). Adaptive three-phase estimation of sequence components and frequency using hco filter based on sparse model. *J. Mod. power Syst. clean energy* 8, 981–990. doi:10.35833/mpce.2018.000440

Tan, Y., He, Z., and Tian, B. (2015). A novel generalization of modified lms algorithm to fractional order. *IEEE Signal Process. Lett.* 22, 1244–1248. doi:10.1109/lsp.2015.2394301

Wold, J., and Wilches-Bernal, F. (2021). Enhanced nonlinear least squares for power system frequency estimation with phase jump immunity. *Int. J. Electr. Power and Energy Syst.* 129, 106876. doi:10.1016/j.ijepes.2021.106876

Xie, J., Wei, X., Bo, X., Zhang, P., Chen, P., Hao, W., et al. (2023). State of charge estimation of lithium-ion battery based on extended kalman filter algorithm. *Front. Energy Res.* 11, 1180881. doi:10.3389/fenrg.2023.1180881

Xu, L., and Song, G. (2020). A recursive parameter estimation algorithm for modeling signals with multi-frequencies. *Circuits, Syst. Signal Process.* 39, 4198–4224. doi:10.1007/s00034-020-01356-3

Zahmoul, R., Ejbali, R., and Zaied, M. (2017). Image encryption based on new beta chaotic maps. *Opt. Lasers Eng.* 96, 39–49. doi:10.1016/j.optlaseng.2017.04.009

Zhang, S., Zhang, J., Zheng, W. X., and So, H. C. (2019). Widely linear complex-valued estimated-input lms algorithm for bias-compensated adaptive filtering with noisy measurements. *IEEE Trans. Signal Process.* 67, 3592–3605. doi:10.1109/tsp.2019.2919412

Zhang, X., Ding, Q., Luo, H., Hui, B., Chang, Z., and Zhang, J. (2017). Infrared small target detection based on directional zero-crossing measure. *Infrared Phys. and Technol.* 87, 113–123. doi:10.1016/j.infrared.2017.09.016

Zhao, J., Gómez-Expósito, A., Netto, M., Mili, L., Abur, A., Terzija, V., et al. (2019). Power system dynamic state estimation: motivations, definitions, methodologies, and future work. *IEEE Trans. Power Syst.* 34, 3188–3198. doi:10.1109/tpwrs.2019.2894769

Zubair, S., Chaudhary, N. I., Khan, Z. A., and Wang, W. (2018). Momentum fractional lms for power signal parameter estimation. *Signal Process.* 142, 441–449. doi:10.1016/j.sigpro.2017.08.009